The worldwide invasion history of a pest ambrosia beetle inferred using population genomics

T. Urvois, C. Perrier, Alain Roques, L. Sauné, C. Courtin, H. Kajimura, J. Hulcr, A. I. Cognato, M.-A. Auger-Rozenberg, C. Kerdelhué

The worldwide invasion history of a pest ambrosia beetle inferred using population genomics

Short title: *Xylosandrus crassiusculus'* invasion history

T. Urvois[1,2], C. Perrier[2], A. Roques[1], L. Sauné[2], C. Courtin[1], H. Kajimura[3], J. Hulcr[4,5], A.I. Cognato[6], M.-A. Auger-Rozenberg[1], C. Kerdelhué[2]

[1] INRAE, URZF, 45075 Orleans, France

[2] UMR CBGP, INRAE, CIRAD, IRD, Institut Agro, Université Montpellier, Montpellier, France

[3] Graduate School of Bioagricultural Sciences, Nagoya University, Nagoya, Japan

[4] School of Forest, Fisheries, and Geomatics Sciences, University of Florida, Gainesville, FL, USA

[5] Department of Entomology and Nematology, University of Florida, Gainesville, FL, USA

[6] Department of Entomology, Michigan State University, East Lansing, MI, USA

Corresponding author mail: teddyurvois@gmail.com

Abstract

Xylosandrus crassiusculus, a fungus-farming wood borer native to Southeastern Asia, is the most rapidly spreading invasive ambrosia species worldwide. Previous studies focusing on its genetic structure suggested the existence of cryptic genetic variation in this species. Yet, these studies used different genetic markers, focused on different geographical areas, and did not include Europe. Our first goal was to determine the worldwide genetic structure of this species based on both mitochondrial and genomic markers. Our second goal was to study *X. crassiusculus'* invasion history on a global level and identify the origins of the invasion in Europe. We used a COI and RAD sequencing design to characterize 188 and 206 specimens worldwide, building the most comprehensive genetic dataset for any ambrosia beetle to date. The results were largely consistent between markers. Two differentiated genetic clusters were invasive, albeit in different regions of the world. The two markers were inconsistent only for a few specimens found exclusively in Japan. Mainland USA could have acted as a source for further expansion to Canada and Argentina through stepping-stone expansion and bridgehead events. We showed that Europe was only colonized by Cluster 2 through a complex invasion history including several arrivals from multiple origins in the native area, and possibly including bridgehead from the USA. Our results also suggested that Spain

30   was colonized directly from Italy through intracontinental dispersion. It is unclear whether the mutually

31   exclusive allopatric distribution of the two Clusters is due to neutral effects or due to different ecological

32   requirements.

35

36   Introduction

37   The number of biological invasions has increased in the last decades and is still increasing (Seebens

38   et al. 2017, Sardain et al. 2019). Invasions are known to potentially have harmful effects on native

39   biodiversity and ecosystems (Kenis et al. 2008, Simberloff et al. 2013) as well as on anthropized ecosystems

40   (Paini et al. 2016) and human health (Jones and McDermott 2017). Invasion scenarios are diverse, ranging

41   from a single introduction event (Hughes et al. 2017) to more complex histories implying multiple

42   introductions and/or multiple sources (Javal et al. 2019, Tang et al. 2022). Moreover, invaded regions can act

43   as sources for invasions to subsequent regions, a phenomenon called "bridgehead effect" (Lombaert et al.

44   2010, Bertelsmeier et al. 2021). Invasion history shapes the invasive populations' genetic structure and

45   diversity, which can affect the invasion dynamics. For example, invasions starting with a limited number of

46   individuals and a low diversity of genotypes may result in significant genetic load and low evolutionary

47   potential in the established populations (Schrieber and Lachmuth 2017). Identifying invasion routes and

48   patterns of genetic structure and diversity are thus crucial to understand the demographic and genetic

49   processes occurring in invasive populations and predict their progression, and to prevent further

50   introductions via the identification of sources and points of entry. Studying worldwide genetic structure of

51   invasive species can be considered as the most effective way to understand species' invasion history (Estoup

52   and Guillemaud 2010).

53   Studying population genetic structure of an invasive species can also reveal the existence of cryptic

54   species or infraspecific genetic differentiation. Such information is crucial, as it can change the taxonomic

55   scale at which the invasion should be considered and managed. For example, the *Euwallacea fornicatus*

56   species complex was considered a single species when it was first described outside its native area, but is

57   now considered to comprise seven species with overlapping morphologies (Smith et al. 2019). Studying its

58   population genetic structure in Hawaii revealed the co-occurrence of two species of the complex (Rugman-

59 Jones et al. 2020). Such findings can affect detection protocols and management decisions, for example, by

60 helping find suitable natural enemies for biological control (Stouthamer et al. 2017). Information on

61 infraspecific divergence is also essential, as different genetic lineages can have different biotic and abiotic

62 preferences. Differentiated clades can have different potential distributions (Godefroid et al. 2015), potential

63 impacts (e.g., if they preferentially attack different host plants) and origins.

64   The ambrosia beetles from the Xyleborini tribe are remarkable invaders, which can be explained by

65 several biological characteristics (Hulcr and Stelinski 2017). They are minute species and they live inside

66 galleries in their host plants. Hence they can be easily transported over long distances inside their hosts with

67 international trade and escape sanitary inspections and treatments. They are xylomycetophagous (i.e. they

68 feed on their symbiotic fungus rather than directly from the host plant tissues), which allows them to attack a

69 broad range of host plant species. They are haplodiploid (i.e. haploid males hatch from non-fertilized eggs,

70 while diploid females hatch from fertilized eggs), and they have a sib-mating reproduction, usually directly

71 in their maternal galleries. This has several consequences. First, their genome is expected to be constantly

72 purged from deleterious mutations, lowering the risk of inbreeding depression often observed in small

73 invasive populations. Consistently, outbreeding depression but not inbreeding depression was previously

74 documented in a species of ambrosia beetles (*Xylosandrus germanus*) (Peer and Taborsky 2005). Second, it

75 eases mate finding even in very small populations, as during invasions. Lastly, haplodiploidy combined with

76 their adult longevity allow single unmated females to establish a population, by mating with their male

77 offsprings (produced from unfertilized eggs) to give a second generation comprising both haploid males and

78 diploid females. Despite the damage caused by ambrosia beetles, the number of studies on their invasion

79 history remains very limited. Kajtoch et al. (2022) reported less than 40 studies on saproxylic beetles'

80 phylogeography, and a particular lack of data for tropical and subtropical areas.

81   *Xylosandrus crassiusculus* is an ambrosia beetle originating from Southeastern Asia which is

82 invasive worldwide. As opposed to most ambrosia beetles, *X. crassiusculus* attacks weakened and stressed

83 trees in its invaded area, including fruit trees such as avocado (*Persea americana*) (Regupathy and

84 Ayyasamy 2014), economically important crops such as cocoa (*Theobroma cacao*), coffee (*Coffea arabica*)

85 and tea (*Camellia sinensis*), and ornamental trees such as *Cercis siliquastrum* (Kavčič and de Groot 2017). It

86 invaded Africa more than a century ago (Hagedorn 1908, Schedl 1953), Pacific islands in 1950 (Samuelson

87   1981), North America in 1974 (Anderson 1974), South America in 2001 (Kirkendall 2018), and was

88   detected in Europe recently, first in Italy in 2003 (Pennachio et al. 2003) and then in various European

89   countries (France in 2014 (Roques et al. 2019), Spain in 2016 (Gallego et al. 2017), and Slovenia in 2017

90   (Kavčič 2018)). Several studies have already focused on *X. crassiusculus*' genetic structure and

91   phylogeography and suggested the existence of two genetically differentiated clusters (Dole et al. 2010,

92   Landi et al. 2017, Storer et al. 2017, Nel et al. 2020). Ito and Kajimura (2009), focusing only on its native

93   area in Japan, identified three distinct mitochondrial lineages. Despite these studies, the complete invasion

94   picture remains unclear as the authors used different genetic markers, focused on different geographical

95   areas, and did not include the European population.

96   This study aimed to characterize *Xylosandrus crassiusculus*' genetic structure and decipher its

97   worldwide invasion history. We used both a mitochondrial marker and pangenomic nuclear markers, as they

98   can provide complementary information because they are differently inherited and do not evolve at the same

99   rate (Toews and Brelsford 2012).

100   This approach will reconcile the results obtained in the previously published including individuals

101   from Japanese clades and sub-clades (Ito & Kajimura (2009) and from the same regions as in Storer et al.

102   (2017). Furthermore, we used the same mitochondrial fragment as in Landi et al. (2017) and Nel et al. (2020)

103   so to include their data in our global analysis.

104   Our first goal was to compare the genetic structure based on the mitochondrial and nuclear markers

105   and to determine whether they conformed to previous patterns, such as the two highly differentiated clusters

106   identified worldwide by Storer et al. (2017) or the three mitochondrial lineages observed in Japan by Ito and

107   Kajimura (2009). Our second goal was to study the invasion history of the species on a global-level,

108   including the invasive populations in Europe. Specifically, we aimed to identify the origin(s) of the invasion

109   in Europe, to determine whether it was invaded by several sources and whether bridgehead events occurred.

110   Material & Methods

111   Insect sampling

112   We assembled *Xylosandrus crassiusculus* females from 64 localities (Table 1, Supplementary Table

113   1), 31 localities in five countries in its native range and 33 localities in nine countries distributed on three

114   continents in invaded ranges. While *X. crassiusculus* is often described as native to Eastern and Southeastern

115   Asia (Ito and Kajimura 2009, Ranger et al. 2016, Gallego et al. 2017), the precise boundaries of its native

116 range are unknown. We thus decided to consider all Asian localities as part of *X. crassiusculus* native area.

117 The insects were either collected directly from the host tree, using traps baited with ethanol or more specific

118 attractants (Roques et al., in prep), or obtained from collaborators. Whenever possible, individuals from the

119 same location were selected as to minimize inter-individual relatedness within each location, by choosing

120 different source trees or collections from different days. Individuals were stored in 96% ethanol and at -18°C

121 until DNA extraction.

122 DNA extraction

123 To reduce expected contamination by symbiotic and non-symbiotic fungi, specimens first had their

124 mycangia removed, were then washed with 70% alcohol and were cleaned with a paintbrush. DNA was then

125 individually extracted using the Macherey-Nagel NucleoSpin Tissue kit following the manufacturer's

126 instructions except with two successive elutions in 50 µL BE buffer, and then stored at -18°C.

127 Mitochondrial DNA sequencing and statistical analyses

128 We sequenced 188 specimens, 72 from the native area and 116 from the invaded range (Table 1,

129 Supplementary Table 1), using between one and 16 insects per location. Specimens obtained from Japan

130 originated from the same populations as in Ito and Kajimura (2009). We amplified the barcode COI

131 fragment via PCR using the primers HCO2198 (5' –TAAACTTCAGGGTGACCAAAAAATCA – 3') and

132 LCO1490 (5' – GGTCAACAAATCATAAAGATATTGG – 3') (Folmer et al. 1994). The PCR was

133 performed as follows: denaturation for 5 min at 94°C followed by 35 cycles of amplification of 45 sec at

134 94°C, 50 sec at 47°C and 90 sec at 72°C and finally 5 min at 72°C. PCR products were cleaned using the

135 NucleoSpin Gel and PCR Cleanup kit (Machery-Nagel) and sequenced in both directions using the ABI

136 Prism BigDye Terminator v3.1 Cycle Sequencing Kit on an ABI Prism 3500 Genetic Analyzer (Thermo

137 Fisher Scientific). We used CodonCode (CodonCode Corporation) to check electropherograms, create

138 contigs and trim all sequences to 567 bp. DNA sequences were aligned using ClustalW in MEGA X (Kumar

139 et al. 2018). We completed the alignment with all of the barcode COI sequences publicly available from

140 Genbank and for which location information was available, i.e., 32 sequences from 24 localities in 11

141 countries, including sequences from Cognato et al. (2020) (MN620070.1-MN620078.1), Dole et al. (2010)

142 (GU808708.1-GU808711.1), Ramage et al. (2017) (KX055192.1-KX055198.1), Landi et al. (2017)

143 (KX685266.1), Sire et al. (2019) (MN182983.1, MN183016.1) and Nel et al. (2020) (MT230099.1,

144 MT230101.1, MT230103.1, MT230104.1). The final alignment included 220 individuals.

145 Mitochondrial data statistical analysis

146   We calculated Kimura 2 Parameters (K2P) and p genetic distances between haplotypes and clusters

147 using MEGA X (Kumar et al. 2018). Haplotype and nucleotide diversities were calculated using the pegas

148 package (Paradis 2010) in the R Software (R Core Team 2018). We reconstructed a phylogeny between

149 haplotypes using Maximum-Likelihood and Bayesian inference, with *Xylosandrus germanus* and *X.*

150 *morigerus* (accession numbers NC_036280.1 and NC_036283.1, respectively). A Maximum-Likelihood

151 phylogeny was performed with MEGA X (Kumar et al. 2018) with 1000 bootstraps using K2P distances. A

152 Bayesian inference of the haplotype phylogeny was performed with MrBayes (Ronquist et al. 2012) with a

153 GTR + I + Γ evolutionary model, and 4 chains run 4 times during 2,000,000 generations with a diagnostic

154 every 100 generations. A median-joining network was realized with PopArt (Bandelt et al. 1999). Lineage

155 and haplotype maps were performed using the R packages maps (Becker et al. 2018), ggplot2 (Wickham

156 2016) and scatterpie (Guangchuang 2020).

157 RAD sequencing and bioinformatics

158   DNA quantity and quality were assessed using the Qubit dsDNA HS Assay Kit with a Qubit

159 fluorometer. As previously found for the closely related species *Xylosandrus compactus* (Urvois et al. 2022),

160 the DNA amount extracted here from each individual of *Xylosandrus crassiusculus* was too small to allow

161 the direct construction of RAD libraries, therefore we carried out whole genome amplification. We used the

162 Genomiphi kit V3 following the manufacturer's procedure and the protocol used by Cruaud et al. (2018).

163 Individual RAD libraries were then constructed following Baird et al. (2008) and Etter et al. (2011) with a

164 few modifications listed hereafter. DNA was digested using 250 ng of DNA in 22 µL per sample and 0.5 µL

165 of the PstI-HF enzyme for a total volume of 25 µL. The digested fragments from each specimen were tagged

166 with a unique 5- or 6- bp barcode and a P1 adapter using 1.5 µL of P1 adapter (100 nM) and 0.5 µL of T4

167 Ligase (2.000.000 U/ml) for a total volume of 30.5 µL. Specimens were then pooled 32 by 32 to create

168 seven libraries. Libraries were sonicated on a Covaris S220 (duty cycle 10%, intensity 5, 200 cycles/burst,

169 duration 75 s) to obtain 300-600 bp fragments. Each library was then tagged with a 5- or 6- nucleotide

170 barcode and a P2 adapter using 1 µL of P2 adapter (10 nM) and 0.5 µL of Quick Ligase (2,000,000 U/ml).

171 The sizing and purification steps were realized using AMPure XP beads (Agencourt). We performed 5 PCR

172 enrichment with 15 cycles (30 ng DNA input, NEB Phusion High-Fidelity PCR Master Mix) for each library

173   to increase fragment diversity. After quality control using the Agilent 2100 Bioanalyzer, the libraries were

174   pooled altogether at an equimolar ratio and sent to MGX-Montpellier GenomiX for sequencing. The library

175   was verified on a Fragment Analyser (Agilent, HS NGS fragment Kit), quantified by qPCR (Kapa Library

176   quantification kit) and sequenced on a SP lane in paired-end 2 x 150 nt mode on a Novaseq6000 (Illumina)

177   according to the manufacturer's instructions.

178   We used the RADIS pipeline (Cruaud et al. 2016) to demultiplex individuals using process_radtags

179   (Catchen et al. 2013) and to remove a few low-quality bases at the 3'-ends by trimming all reads at 139 bp.

180   Some specimens were not used in the analysis due to the poor quality of the sequences, leaving between 1

181   and 7 insects per location for a total of 206 specimens, 81 from the native area and 125 from the invaded

182   range (Table 1, Supplementary Table 1). We obtained on average 7,162,285 (2,534,799 SD) reads per

183   specimen after demultiplexing. We then removed PCR duplicates using clone_filter (Catchen et al. 2013),

184   decreasing the number of reads per individual to 2,323,533 (801,285 SD) on average. To remove potential

185   human DNA contaminations (which can occur during whole genome amplification), we aligned the

186   remaining reads on the reference genome GRCh38.p13 of *Homo sapiens* (accession number:

187   GCA_000001405.28) using the BWA-MEM algorithm (Li and Durbin 2009) and we removed the 103,074

188   mapping reads, thereby keeping 2,220,459 (785,925 SD) reads per specimen on average.

189   The following steps were performed using STACKS (Catchen et al. 2013, Rochette et al. 2019) on

190   the Genotoul Bioinformatics Platform (INRAE, Toulouse, France). We ran a pre-analysis on 20 specimens

191   selected to encompass a maximum of genomic diversity to assess the effect of 9 combinations of M and n

192   parameters in STACKS modules: M = 6, 8 and 10 in ustacks (i.e. the maximum distance allowed between

193   stacks) and n = 4, 6 and 8 in cstacks (i.e. the number of mismatches allowed between sample loci when

194   building the catalogue). To remove potential fungal contaminations, we then aligned the obtained loci on the

195   *Ambrosiella xylebori*'s reference genome (accession number: ASM277803v1 (Vanderpool et al. 2018)), as it

196   was the closest complete reference genome available to *X. crassiusculus*' symbiotic fungus. We used the

197   BWA-MEM algorithm (Li and Durbin 2009) to create a list of potential fungal reads, mapping on the

198   *Ambrosiella xylebori*'s genome, to be later removed in STACKS' *populations* module. Between 0.14% and

199   0.16% of the sequences mapped on the *Ambrosiella xylebori*'s genome, depending on the combinations of

200   the parameters M and n, and were all listed to be removed. In STACKS' *populations* module, we used three

201   possible filtering values for parameter r (the minimum percentage of individuals required to process a locus,

202   here with one population), r = 0, 0.3 and 0.7, respectively. We excluded loci obtained with a mean read depth

203   lower than 8 using VCFtools (Danecek et al. 2011) to test the effect of depth filtering. We compared the

204   number of SNPs and the individual mean depth, homozygosity and missing data for each M, n and r

205   combination. For each combination, we also performed clustering with SNPrelate (Zheng et al. 2012) and

206   used the dendextend R package (Galili 2015) to untangle the obtained dendrograms using the "step1side"

207   method and calculate their entanglement using the entanglement function. The combination of the

208   parameters M and n had limited effects on our results. For a given r, each parameter combination of M and n

209   yielded similar numbers of SNPs (Supplementary Table 2), individual mean depth, homozygosity and

210   missing data (Supplementary Figures S1, S2 & S3), and tree topologies were identical for every parameters

211   combination (Supplementary Figures S4 & S5). Following this pre-analysis, we launched the analysis of the

212   complete dataset, using M = 6, n = 4, and r = 0.8, excluding loci matching *X. crassiusculus*' symbiotic fungi,

213   and removing loci with a mean depth lower than 8. This M and n parameter set corresponded to the

214   parameters used for *X. compactus* in Urvois et al. (2022). We finally obtained a dataset of 83,055 filtered

215   SNPs.

RAD SNP statistical analysis

217   We estimated the specimens' relative ancestry using Admixture (Alexander et al. 2009), with a

218   putative number of populations, K, ranging from 2 to 20 with a 100-fold cross-validation to assess the best K.

219   We then used the pong 1.4.9 software (Behr et al. 2016) to estimate the major mode (using a greedy

220   approach with 300 runs and a similarity threshold value of 0.95), and plotted and mapped the results using

221   the ggplot2 package (Wickham 2016) in the R Software (R Core Team 2018). A Maximum Likelihood tree

222   was generated using RAxML 8.2.21 (Stamatakis 2014). We used the GTRCAT approximation and allowed

223   the program to automatically halt bootstrapping using the bootstrap converge criterion (Pattengale et al.

224   2010) through the autoMRE option. The tree was visualized using FigTree V.1.4.4

225   (https://github.com/rambaut/figtree/releases). Besides, a hierarchical clustering tree was built using

226   SNPRelate (Zheng et al. 2012) on an individual dissimilarity matrix (Zheng 2013). We also calculated, using

227   the StAMPP package (Pembleton et al. 2013), the pairwise Fst (Wright 1951, Weir and Cockerham 1984)

228   and Nei distances (Nei 1972) between the different genomic groups previously obtained with Admixture.

Results

Mitochondrial diversity and differentiation

229 Results

230 Mitochondrial diversity and differentiation

231 We obtained 50 mitochondrial haplotypes worldwide (Table 1, Figure 1), with 139/567 variable base

232 pairs. Haplotype and nucleotide diversities were 0.954 and 0.074 in the native area and 0.795 and 0.045 in

233 the invaded area, respectively. We found 41 haplotypes in *X. crassiusculus*' native area, including 16 in

234 Japan, 12 in Vietnam, 11 in China, two in Taiwan, one in India, one in Indonesia and one in Thailand. We

235 found 13 haplotypes in *X. crassiusculus*' invasive range, including five in Hawaii, four in mainland USA,

236 two in mainland France, American Samoa, French Guiana, French Polynesia, South Africa and Slovenia,

237 and one in Argentina, Canada, Italy, Madagascar, New Zealand, Panama and Spain. Three haplotypes were

238 present in more than four localities (A02, A10 and D02, Figure 1), whereas 36 haplotypes were only found

239 in one locality. Four haplotypes were found in both the native and the invasive areas (A02, A07, A10, D02)

240 (Table 1, Figure 1, Supplementary Table 1). Haplotype A02 was the most widespread haplotype, found in 26

241 localities in 8 countries (Japan in the native range, and Papua New Guinea, Argentina, Canada, Italy, New

242 Zealand, Spain and the USA in the invasive area). Haplotype D02 was identified in 12 localities in six

243 countries (Indonesia and Japan in the native area, and Papua New Guinea, Madagascar and the Pacific

244 Islands of France and the USA in the invasive area). Haplotype A10 was found in 14 localities in four

245 countries (China, France, Slovenia and the USA), and haplotype A07 was found in two localities in Japan

246 and the USA. The median-joining network showed that five haplotypes (A01, A03, A08, D03 and D04) that

247 were private to the invasive range had a single mutational step from haplotypes found in the native range

248 (Supplementary Figures S6 & S7). Haplotype D10 was three mutational steps away from D09. The

249 haplotype A11 was the closest to the three remaining invasive haplotypes A05, A06, and A09 with 3, 4 and 7

250 mutational steps, respectively.

251 The Maximum-Likelihood and the Bayesian inference trees suggested that haplotypes can be

252 grouped in two differentiated Clusters (Figure 2, Supplementary Figures S8 & S9) generally consistent with

253 the results found by Storer et al. (2017). The average K2P and p genetic distances within Clusters were

254 0.054 (0.032 Standard Error Estimate) and 0.050 (0.010 SEE), and between Clusters of 0.118 (0.008 SEE)

255 and 0.109 (0.010 SEE), respectively (Supplementary Table 3). Both Clusters were further structured into

256 five mitochondrial lineages, Cluster 1 including lineages D and E, and Cluster 2 including lineages A, B and

257 C (Table 1, Figures 3, Supplementary Figure S8). To ease the comparison of results across studies, our

258   lineages A, B and C fully correspond to the lineages A, B and C already identified in Ito and Kajimura's

259   study (2009), and we named D and E the two new mitochondrial lineages we identified in the present work.

260   The K2P distances within lineages were lower than 0.049 (mean 0.020) (Table 1) and between lineages

261   higher than 0.070 (mean 0.103) (Table 2). Lineage A comprised 12 haplotypes and was present in the native

262   area in China and Japan, and in the invaded area in France, Italy, Slovenia, Spain, Argentina, New Zealand,

263   Papua New Guinea, Canada, mainland USA and Hawaii (Figure 3). Lineages B and C were exclusively

264   found in Japan and consisted of 7 and 6 haplotypes, respectively. Lineage D comprised 10 haplotypes and

265   was found in the native area in China, India, Indonesia, Japan, Thailand, Vietnam, and in the invaded area in

266   Papua New Guinea, Madagascar, Panama, French Polynesia, Hawaii, American Samoa and French Guiana.

267   Finally, lineage E was composed of 15 haplotypes and was found exclusively in *X. crassiusculus*' native area

268   in China, Taiwan and Vietnam. The Maximum-Likelihood tree reached high support (>0.50) for most nodes

269   except for some nodes within lineage A and within lineage E (Figure 2). On the other hand, the Bayesian

270   inference tree had a lower resolution and had low support for the separation between lineages A and B

271   (Posterior Probability = 0.78) but high support for lineages C, D, and E (Supplementary Figure S9).

272   Genetic structure at nuclear SNPs obtained from RAD sequencing

273   The average homozygosity estimated from RADseq data was 0.993 (0.016 SD), and the average

274   inbreeding coefficient was 0.958 (0.101 SD). When running Admixture on the complete dataset, the cross-

275   validation values reached a plateau for K = 9, which we considered the most parsimonious number of

276   genomic groups (Supplementary Figure S10). With a similarity threshold of 0.95, the 300 Admixture runs

277   yielded 82 modes, the major mode representing 109 runs with a pairwise similarity of 0.978.

278   The genomic groups obtained at K = 2 matched the mitochondrial Clusters 1 and 2 for most

279   individuals, except for 17 specimens showing a low assignation score and corresponding to the

280   mitochondrial lineages B and C (Supplementary Figure S11) from Japan. These particular specimens formed

281   the third genomic group at K = 3 (Figure 4), the two other genomic groups corresponding to (i) all the

282   individuals of the mitochondrial Cluster 1, and (ii) the individuals of Cluster 2 restricted to the lineage A

283   described above (Figure 4). We will hereafter refer to these three groups as Cluster JapB-C and genomic

284   Clusters 1 and 2 (Figure 4). For the optimal K = 9, the Cluster JapB-C was further split into the genomic

285   groups 1 and 2 (tightly corresponding to the mitochondrial lineages B and C mentioned above), genomic

286   Cluster 2 was composed of the genomic groups 3, 4 and 5 (including all individuals from the mitochondrial

287   lineage A) and genomic Cluster 1 comprised the genomic groups 6, 7, 8 (corresponding to mitochondrial

288   lineage D) and 9 (mitochondrial lineage E).

289   For K = 9, 177 specimens were assigned to their genomic group with a score higher than 0.95, and

290   154 scored more than 0.999. Within genomic Cluster 1, two groups were restricted to the native area

291   (genomic group 6 occurred only in one locality in China and genomic group 9 was present in Taiwan,

292   Vietnam and China (Figure 5)), and two groups were invasive in different regions of the world (genomic

293   group 7 was native from Indonesia and invasive in the Pacific Islands, Costa Rica, French Guiana and Papua

294   New Guinea; genomic group 8 was native from Vietnam and invasive in Papua New Guinea and Vietnam).

295   Within genomic Cluster 2, the three identified genomic groups were found both in native and invasive areas.

296   Group 3 was found in Japan (native area) and Hawaii, mainland USA, Spain, Italy, New Zealand and Papua

297   New Guinea in the invaded area (Figure 6). Genomic group 4 was found in Japan and China in the native

298   range, and in Italy, France, Slovenia, , Hawaii and mainland USA in the invasive regions. Note that some

299   specimens from the USA were assigned as admixed between genomic groups 3 and 4. Genomic group 5 was

300   composed exclusively of specimens from France and one specimen from Costa Rica, and was thereby not

301   found in the native range.

302   The Fst and Nei distances between genomic Clusters were 0.956 and 0.366, respectively (Table 3).

303   Between genomic groups, they averaged 0.894 (0.125 SD) and 0.294 (0.132 SD), respectively. Our results

304   showed a lower divergence between genomic groups within Cluster 2 than within Cluster 1, with average

305   Fst of 0.529 (0.0132 SD) and 0.847 (0.059 SD), and Nei distances of 0.0189 (0.005 SD) and 0.102 (0.020

306   SD), respectively.

307

308   The RAxML analysis stopped after 400 bootstraps with a best tree scoring a likelihood score of -

309   359,651.47. The phylogenetic tree was very consistent with the clustering tree and Admixture results

310   described above. It revealed two groups corresponding to the Cluster JapB-C (Admixture groups 1 and 2)

311   and two distinct Clusters corresponding to the genomic Clusters 1 and 2, respectively split in 4 and 3 major

312   branches (Supplementary Figure S12) matching groups 6 to 9 on the one hand, and groups 3 to 5 on the

313   other hand.

314

Discussion

The aim of this study was to analyze the genetic structure and the invasion history of *X. crassiusculus* worldwide, using a strategy that reconciled previous studies (which used different markers and focused on different regions) and to obtain a global picture including previously unstudied areas such as Europe. To do so, we sequenced the barcode mitochondrial marker in all regions, which allowed us to merge the data previously published from South America and South Africa and sequences retrieved from GenBank. We included a subset of the individuals studied in Ito & Kajimura (2009) corresponding to all the clades and subclades they identified using the second half of the COI gene (i.e., a fragment which did not overlap with the barcode region), which allowed for an interpretation of our results in the light of the Japanese genetic structure. Finally, we also included specimens from the main regions studied in Storer et al. (2017) which allowed for an evaluation of the consistency between their results and ours. This sampling design and the use of both mitochondrial and nuclear pangenomic markers provided a broader view of the genetic structure and of the dispersal around the globe.

To facilitate the comparisons between studies, we named the main genetic groups and lineages consistently with previous results, in particular our mitochondrial clusters A, B and C corresponded to the clusters identified by Ito and Kajimura (2009) under the same codes. Both mitochondrial and nuclear markers highlighted the existence of two main genetic Clusters that were generally consistent with the results found by Storer et al. (2017). The same genetic groups in our study and theirs are consistently named Cluster 1 and Cluster 2.

Genetic structure in *Xylosandrus crassiusculus*
The consolidated global genetic structure of X. crassiusculus

Most individuals fall into two main highly differentiated genetic clusters supported both by mitochondrial and nuclear data, in this as well as in previous studies. Interestingly, Clusters are mostly allopatric and overlap only in a few regions (Figure 7). Cluster 1 is native to China, India, Indonesia, Taiwan, Thailand (Storer et al. 2017) and Vietnam, and was found once in Okinawa (Storer et al. 2017, Cognato et al. 2020). It is invasive in Papua New Guinea, Central America, the Pacific islands, and several African countries (Storer et al. 2017, Nel et al. 2020). Cluster 2 is native to China, Japan and Taiwan (Ito and Kajimura 2009, Storer et al. 2017), and invasive in South, Central, and North America (Storer et al. 2017), in the Pacific Islands, Africa (Nel et al. 2020), Oceania and Europe. The two Clusters were only found together

344   in the native area in Taiwan (Storer et al. 2017), the Guangxi province in China and Okinawa. In the invaded

345   range, they co-occurred in O'ahu Island in Hawaii, in Papua New Guinea and in South Africa. Both Clusters

346   were also found in Central America, but each in a different country. Moreover, their worldwide distributions

347   suggest that Cluster 1 had a circumtropical distribution while Cluster 2 was present at higher latitudes and in

348   temperate regions. The apparent difference between the two Clusters' geographical distributions may

349   associate with various factors such as different abiotic requirements (i.e., climatic requirements), different

350   biotic interactions (i.e., host association) or different colonizable ranges due, for instance, to different means

351   of passive transportation (Guisan et al. 2017). Tests of these hypotheses will require additional sampling and

352   specific analyses.

353

354   *Mitonuclear discordance in one clade found in Japan*

355   Most specimens could be unambiguously assigned to one of the two main genetic Clusters discussed

356   above. Still, a group of 17 individuals found exclusively in Japan (mitochondrial lineages B and C, this

357   study and Ito & Kajimura (2009)) were placed in a third genomic Cluster we called JapB-C. However, these

358   individuals were phylogenetically close to the ones belonging to mitochondrial lineage A and were thus

359   expected to belong to Cluster 2. Such a discrepancy between markers is referred to as a case of mitonuclear

360   discordance. It can result from diverse phenomena, including natural selection, introgression, sex-bias in

361   offsprings, sex-biased dispersal (El Mokhefi et al. 2016) or reproductive manipulation by *Wolbachia* (Sloan

362   et al. 2017). Still, it is beyond the scope of this study to investigate the cause of the observed differences.

363

364   *Xylosandrus crassiusculus*' invasion history and pathways

365   Our study is the first to include specimens from Europe. Europe was only invaded by Cluster 2, with

366   specimens from the three genomic groups (3, 4 and 5), and four haplotypes from the mitochondrial lineage

367   A. The closely related species *X. germanus* (Dzurenko et al. 2020) and *X. compactus* (Urvois et al. 2022)

368   seem to have spread across Europe from single introductions, but *Xylosandrus crassiusculus*' likely invaded

369   Europe multiple times from multiple sources, followed by local dispersal as observed for other xyleborine

370   species in North America (Cognato et al. 2015, Smith and Cognato 2022). The first invaded Italian locality

371   among our sampling sites (Circeo National Park) is characterized by haplotype A02 and the genomic group

372   3. This could point to a source in Japan if the species was directly introduced from the native range, or to a

373 source in the US, as several North American localities invaded during the 20th century had the same genetic

374 characteristics (Figure 8). Spanish populations were genetically very similar to the Italian ones, suggesting

375 that *X. crassiusculus* colonized Spain directly from the Italian source through intracontinental movements.

376 Bridgehead events from the USA to Europe were already documented for various invasive insect species, for

377 example, *Harmonia axyridis* (Lombaert et al. 2010), *Leptoglossus occidentalis* (Lesieur et al. 2018) or

378 *Anoplophora glabripennis* (Javal et al. 2019).

379   Specimens from Southeastern France bore haplotype A10, also found in Shanghai in the native area.

380 This suggests an independent colonization event from the region of Shanghai, similar to *X. compactus*

381 (Urvois et al. 2022). However, as Shanghai is one of China's most economically important cities and the

382 busiest port worldwide (UNCTAD 2020), it could also have acted as a bridgehead by exporting infested

383 plants coming from other areas in China or other countries in Asia, as observed for the invasive box tree

384 moth *Cydalima perspectalis* by Bras et al. (2019). A few individuals with similar genetic characteristics

385 were found in various European localities where *X. crassiusculus* was later detected, as in Eastern Slovenia,

386 Southern France and Southwestern France, suggesting stepping-stone expansion from Southeastern France

387 to nearby regions. Other European specimens could correspond to other independent colonizations, such as

388 specimens belonging to genomic group 4 with haplotype A02 in Italy or A03 in Southwestern France, or

389 specimens with haplotype A9 in Slovenia. These genetic combinations were not identified in the native or

390 invaded areas, we thus cannot infer the source of these populations.

391

392   Our results also brought complementary information to document the invasion history of *X.*

393 *crassiusculus* in the Americas and Africa. Despite extensive sampling, Storer et al. (2017) exclusively found

394 Cluster 2 in the USA, which agrees with our results. The presence of genomic group 3 and haplotypes A02

395 and A07 in the USA suggests that Japan could be the donor area, similar to the introduction of *X. germanus*

396 to the USA (Dzurenko et al. 2020). Several localities in the USA across different states were genetically

397 similar, and the same mitochondrial haplotype (A02) was found in localities in the USA, Canada and

398 Argentina. We thus hypothesize that mainland USA could have acted as a source for further expansion to

399 Canada and Argentina through stepping-stone expansion and bridgehead events. Storer et al. (2017) reported

400 Africa was invaded from mainland Asia (Cluster 1) and suggested that historic dispersal could explain the

401 high differentiation between Madagascar and other African locations. Our analysis showed that the

402 haplotypes reported by Nel et al. (2020) in South Africa belonged to both Clusters. A similar situation was

403 reported for *Euwallacea fornicatus* with two divergent haplogroups, potentially corresponding to cryptic

404 species, co-occurring in South Africa (Bierman et al. 2022). The seemingly special place of South Africa on

405 the African continent could result from larger imports or traffic due to some of the largest African ports, such

406 as Port Durban or Port of Richards Bay. However, it is also possible that both Clusters also co-occur in other

407 African countries as the sampling in Africa remains very limited. Indeed, *X. crassiusculus* was reported in

408 15 African countries (Nel et al. 2020), but few specimens were sampled in only four of them.

409

410 Monitoring *Xylosandrus crassiusculus*' Clusters in the invaded area

411 Our study confirmed that *X. crassiusculus* comprises at least three differentiated genomic clusters,

412 two of which are invasive worldwide. The strong intraspecific differentiation documented from nuclear and

413 mitochondrial markers and the existence of the Cluster JapB-C suggest a reassessment of potential species

414 limits within *X. crassiusculus*. The p distance between Clusters 1 and 2 based on COI obtained in this study

415 was 10.9% (Standard Error Estimate = 1.0%), fitting in the range reported by Cognato et al. (2020) for the

416 probable recognition of new species of Xyleborini (>10-12% COI and/or >2-3% using the nuclear CAD

417 gene). Other criteria could help rule on the Clusters' status, such as existing gene flow or differences in their

418 ecology. While most specimens were unambiguously assigned to one genomic Cluster for K = 3, the few

419 specimens partly assigned to both Clusters could suggest existing hybridization. Our study also showed that

420 most regions of the world had only one Cluster, suggesting differences in the Clusters' ecological

421 preferences.

422

423 We call for future research comparing the two Clusters' biology and ecology. In case of ecological

424 differences, detecting the arrival of a so far non-occurring Cluster in already invaded areas would be crucial

425 information. The newly introduced Cluster could have a different invasion dynamic, establishing in localities

426 with unsuitable conditions for the other Cluster, attacking new host tree species, or having different

427 phenology with a higher voltinism. In turn, surveillance should be maintained in already invaded countries

428 and genetic expertise should be deployed to identify the intercepted specimens at the Cluster scale and

429 possibly detect the arrival of a so far non-occurring lineage. This early detection would also facilitate the

430 implementation of measures to eradicate populations at their earliest stages (LaBonte 2010), or to control

431 and mitigate the damage caused by *X. crassiusculus* if eradication is not possible.

432

Acknowledgement

442

References

444 Alexander, D. H., J. Novembre, and K. Lange. 2009. Fast model-based estimation of ancestry in unrelated
445 individuals. Genome Research **19**:1655-1664.

446 Anderson, D. M. 1974. First record of *Xyleborus semiopacus* in the continental United States (Coleoptera,
447 Scolytidae). Cooperative Economic Insect Report **24**:863-864.

448 Baird, N. A., P. D. Etter, T. S. Atwood, M. C. Currey, A. L. Shiver, Z. A. Lewis, E. U. Selker, W. A. Cresko,
449 and E. A. Johnson. 2008. Rapid SNP discovery and genetic mapping using sequenced RAD markers.
450 PLoS ONE **3**:e3376.

451 Bandelt, H.-J., P. Forster, and A. Röhl. 1999. Median-joining networks for inferring intraspecific
452 phylogenies. Molecular Biology and Evolution **16**:37-48.

453 Becker, R. A., A. R. Wilks, R. Brownrigg, T. P. Minka, and A. Deckmyn. 2018. maps: draw geographical
454 maps. R package version 3.3.0.

455 Behr, A. A., K. Z. Liu, G. Liu-Fang, P. Nakka, and S. Ramachandran. 2016. pong: fast analysis and
456 visualization of latent clusters in population genetic data. Bioinformatics **32**:2817-2823.

457 Bertelsmeier, C., S. Ollier, and X. Liu. 2021. Bridgehead effects distort global flows of alien species.
458 Diversity and Distributions **27**:2180-2189.

459 Bierman, A., F. Roets, and J. S. Terblanche. 2022. Population structure of the invasive ambrosia beetle,
460 Euwallacea fornicatus, indicates multiple introductions into South Africa. Biological Invasions.

461 Bras, A., D. N. Avtzis, M. Kenis, H. Li, G. Vétek, A. Bernard, C. Courtin, J. Rousselet, A. Roques, and M.-A.
462 Auger-Rozenberg. 2019. A complex invasion story underlies the fast spread of the invasive box tree
463 moth (*Cydalima perspectalis*) across Europe. Journal of Pest Science **92**:1187-1202.

464 Catchen, J., P. A. Hohenlohe, S. Bassham, A. Amores, and W. A. Cresko. 2013. Stacks: an analysis tool set
465 for population genomics. Molecular Ecology **22**:3124-3140.

466 Cognato, A. I., E. R. Hoebeke, H. Kajimura, and S. M. Smith. 2015. History of the Exotic Ambrosia Beetles
467 Euwallacea interjectus and Euwallacea validus (Coleoptera: Curculionidae: Xyleborini) in the United
468 States. Journal of Economic Entomology **108**:1129-1135.

469 Cognato, A. I., G. Sari, S. M. Smith, R. A. Beaver, Y. Li, J. Hulcr, B. H. Jordal, H. Kajimura, C.-S. Lin, T. H.
470   Pham, S. Singh, and W. Sittichaya. 2020. The essential role of taxonomic expertise in the creation of
471   DNA databases for the identification and delimitation of Southeast Asian ambrosia beetle species
472   (Curculionidae: Scolytinae: Xyleborini). Frontiers in Ecology and Evolution **8**.

473 Cruaud, A., M. Gautier, J. P. Rossi, J. Y. Rasplus, and J. Gouzy. 2016. RADIS: analysis of RAD-seq data for
474   interspecific phylogeny. Bioinformatics **32**:3027-3028.

475 Cruaud, A., G. Groussier, G. Genson, L. Saune, A. Polaszek, and J. Y. Rasplus. 2018. Pushing the limits of
476   whole genome amplification: successful sequencing of RADseq library from a single
477   microhymenopteran (Chalcidoidea, Trichogramma). PeerJ **6**:e5640.

478 Danecek, P., A. Auton, G. Abecasis, C. A. Albers, E. Banks, M. A. DePristo, R. E. Handsaker, G. Lunter, G. T.
479   Marth, S. T. Sherry, G. McVean, R. Durbin, and G. Genomes Project Analysis. 2011. The variant call
480   format and VCFtools. Bioinformatics **27**:2156-2158.

481 Dole, S. A., B. H. Jordal, and A. I. Cognato. 2010. Polyphyly of *Xylosandrus* Reitter inferred from nuclear
482   and mitochondrial genes (Coleoptera: Curculionidae: Scolytinae). Molecular Phylogenetics and
483   Evolution **54**:773-782.

484 Dzurenko, M., C. M. Ranger, J. Hulcr, J. Galko, and P. Kaňuch. 2020. Origin of non-native *Xylosandrus*
485   *germanus*, an invasive pest ambrosia beetle in Europe and North America. Journal of Pest Science
486   **94**:553-562.

487 El Mokhefi, M., C. Kerdelhue, C. Burban, A. Battisti, G. Chakali, and M. Simonato. 2016. Genetic
488   differentiation of the pine processionary moth at the southern edge of its range: contrasting patterns
489   between mitochondrial and nuclear markers. Ecology and Evolution **6**:4274-4288.

490 Estoup, A., and T. Guillemaud. 2010. Reconstructing routes of invasion using genetic data: why, how and so
491   what? Molecular Ecology **19**:4113-4130.

492 Etter, P. D., S. Bassham, P. A. Hohenlohe, E. A. Johnson, and W. A. Cresko. 2011. SNP discovery and
493   genotyping for evolutionary genetics using RAD sequencing. Methods in Molecular Biology
494   **772**:157-178.

495 Folmer, O., M. Black, W. Hoeh, R. Lutz, and R. Vrijenhoek. 1994. DNA primers for amplification of
496   mitochondrial cytochrome c oxidase subunit I from diverse metazoan invertebrates. Molecular
497   Marine Biology and Biotechnology **3**:294-299.

498 Galili, T. 2015. dendextend: an R package for visualizing, adjusting and comparing trees of hierarchical
499   clustering. Bioinformatics **31**:3718-3720.

500 Gallego, D., J. L. Lencina, H. Mas, J. Cevero, and M. Faccoli. 2017. First record of the granulate ambrosia
501   beetle, *Xylosandrus crassiusculus* (Coleoptera: Curculionidae, Scolytinae), in the Iberian Peninsula.
502   Zootaxa **4273**:431-434.

503 Godefroid, M., A. Cruaud, J. P. Rossi, and J. Y. Rasplus. 2015. Assessing the risk of invasion by Tephritid
504   fruit flies: intraspecific divergence matters. PLoS ONE **10**:e0135209.

505 Guangchuang, Y. 2020. scatterpie: Scatter Pie Plot. R package version 0.1.5.

506 Guisan, A., W. Thuiller, and N. E. Zimmermann. 2017. Habitat suitability and distribution models with
507   applications in R. Cambridge University Press.

508 Hagedorn, D. E. Z. 1908. *Xyleborus mascarenus*. Deutsche Ent. Zeitschr **379**.

509 Hughes, M. A., J. J. Riggins, F. H. Koch, A. I. Cognato, C. Anderson, J. P. Formby, T. J. Dreaden, R. C.
510   Ploetz, and J. A. Smith. 2017. No rest for the laurels: symbiotic invaders cause unprecedented
511   damage to southern USA forests. Biological Invasions **19**:2143-2157.

512 Hulcr, J., and L. L. Stelinski. 2017. The ambrosia symbiosis: from evolutionary ecology to practical
513   management. Annual Review of Entomology **62**:285-303.

514 Ito, M., and H. Kajimura. 2009. Phylogeography of an ambrosia beetle, *Xylosandrus crassiusculus*
515   (Motschulsky) (Coleoptera: Curculionidae: Scolytinae), in Japan. Applied Entomology and Zoology
516   **44**:549-559.

517 Javal, M., E. Lombaert, T. Tsykun, C. Courtin, C. Kerdelhue, S. Prospero, A. Roques, and G. Roux. 2019.
518   Deciphering the worldwide invasion of the Asian long-horned beetle: A recurrent invasion process
519   from the native area together with a bridgehead effect. Molecular Ecology **28**:951-967.

520 Jones, B. A., and S. M. McDermott. 2017. Health impacts of invasive species through an altered natural
521   environment: assessing air pollution sinks as a causal pathway. Environmental and Resource
522   Economics **71**:23-43.

523 Kajtoch, Ł., M. Gronowska, R. Plewa, M. Kadej, A. Smolis, T. Jaworski, and J. M. Gutowski. 2022. A
524   review of saproxylic beetle intra- and interspecific genetics: current state of the knowledge and
525   perspectives. The European Zoological Journal **89**:481-501.
526 Kavčič, A. 2018. First record of the Asian ambrosia beetle, *Xylosandrus crassiusculus* (Motschulsky)
527   (Coleoptera: Curculionidae, Scolytinae), in Slovenia. Zootaxa **4483**:191-193.
528 Kavčič, A., and M. de Groot. 2017. Pest risk analysis for the Asian Ambrosia Beetle (*Xylosandrus*
529   *crassiusculus* (Motschulsky, 1866)). Slovenian Forestry Institute.
530 Kenis, M., M.-A. Auger-Rozenberg, A. Roques, L. Timms, C. Péré, M. J. W. Cock, J. Settele, S. Augustin,
531   and C. Lopez-Vaamonde. 2008. Ecological effects of invasive alien insects. Biological Invasions
532   **11**:21-45.
533 Kirkendall, L. R. 2018. Invasive bark beetles (Coleoptera, Curculionidae, Scolytinae) in Chile and Argentina,
534   including two species new for South America, and the correct identity of the *Orthotomicus* species in
535   Chile and Argentina. Diversity **10**.
536 Kumar, S., G. Stecher, M. Li, C. Knyaz, and K. Tamura. 2018. MEGA X: Molecular Evolutionary Genetics
537   Analysis across Computing Platforms. Molecular Biology and Evolution **35**:1547-1549.
538 LaBonte, J. R. 2010. Eradication of an exotic ambrosia beetle, *Xylosandrus crassiusculus* (Motschulsky), in
539   Oregon. Pages 41-43 *in* USDA Research Forum on Invasive Species.
540 Landi, L., D. Gómez, C. L. Braccini, V. A. Pereyra, S. M. Smith, and A. E. Marvaldi. 2017. Morphological
541   and molecular identification of the invasive *Xylosandrus crassiusculus* (Coleoptera: Curculionidae:
542   Scolytinae) and its South American range extending into Argentina and Uruguay. Annals of the
543   Entomological Society of America **110**:344-349.
544 Lesieur, V., E. Lombaert, T. Guillemaud, B. Courtial, W. Strong, A. Roques, and M. A. Auger-Rozenberg.
545   2018. The rapid spread of *Leptoglossus occidentalis* in Europe: a bridgehead invasion. Journal of
546   Pest Science **92**:189-200.
547 Li, H., and R. Durbin. 2009. Fast and accurate short read alignment with Burrows-Wheeler transform.
548   Bioinformatics **25**:1754-1760.
549 Lombaert, E., T. Guillemaud, J. M. Cornuet, T. Malausa, B. Facon, and A. Estoup. 2010. Bridgehead effect
550   in the worldwide invasion of the biocontrol harlequin ladybird. PLoS ONE **5**:e9743.
551 Nei, M. 1972. Genetic distance between populations. The American Naturalist **106**:283-292.
552 Nel, W. J., Z. W. De Beer, M. J. Wingfield, and T. A. Duong. 2020. The granulate ambrosia beetle,
553   *Xylosandrus crassiusculus* (Coleoptera: Curculionidae, Scolytinae), and its fungal symbiont found in
554   South Africa. Zootaxa **4838**:zootaxa 4838 4833 4837.
555 Paini, D. R., A. W. Sheppard, D. C. Cook, P. J. De Barro, S. P. Worner, and M. B. Thomas. 2016. Global
556   threat to agriculture from invasive species. Proceedings of the National Academy of Science of the
557   United States of America **113**:7575-7579.
558 Paradis, E. 2010. pegas: an R package for population genetics with an integrated-modular approach. R
559   package version 0.14. Bioinformatics **26**:419-420.
560 Pattengale, N. D., M. Alipour, O. R. Bininda-Emonds, B. M. Moret, and A. Stamatakis. 2010. How many
561   bootstrap replicates are necessary? Journal of Computational Biology **17**:337-354.
562 Peer, K., and M. Taborsky. 2005. Outbreeding depression, but no inbreeding depression in haplodiploid
563   ambrosia beetles with regular sibling mating. Evolution **59**:317-323.
564 Pembleton, L. W., N. O. Cogan, and J. W. Forster. 2013. StAMPP: an R package for calculation of genetic
565   differentiation and structure of mixed-ploidy level populations. Molecular Ecology Resources
566   **13**:946-952.
567 Pennachio, F., P. F. Roversi, V. Francardi, and E. Gatti. 2003. *Xylosandrus crassiusculus* (Motschulsky) a
568   bark beetle new to Europe (Coleoptera Scolytidae). Redia **86**:77-80.
569 R Core Team. 2018. R: a language and environment for statistical computing. R Foundation for Statistical
570   Computing, Vienna, Austria.
571 Ramage, T., P. Martins-Simoes, G. Mialdea, R. Allemand, A. Duplouy, P. Rousse, N. Davies, G. K. Roderick,
572   and S. Charlat. 2017. A DNA barcode-based survey of terrestrial arthropods in the Society Islands of
573   French Polynesia: host diversity within the SymbioCode Project. European Journal of Taxonomy
574   **272**:1-13.
575 Ranger, C. M., M. E. Reding, P. B. Schultz, J. B. Oliver, S. D. Frank, K. M. Addesso, J. Hong Chong, B.
576   Sampson, C. Werle, S. Gill, and C. Krause. 2016. Biology, ecology, and management of nonnative

577   ambrosia beetles (Coleoptera: Curculionidae: Scolytinae) in ornamental plant nurseries. Journal of
578   Integrated Pest Management **7**:1-23.
579 Regupathy, A., and R. Ayyasamy. 2014. Occurrence of ambrosia beetles, *Xylosandrus compactus* (Eichh)
580   and *Xylosandrus crassiusculus* (Motschulsky) on avocado in Tamil Nadu India: pest risk
581   assessment.*in* Pacific Northwest Insect Management Conference, Portland, Oregon, USA.
582 Rochette, N. C., A. G. Rivera-Colon, and J. M. Catchen. 2019. Stacks 2: analytical methods for paired-end
583   sequencing improve RADseq-based population genomics. Molecular Ecology **28**:4737-4754.
584 Ronquist, F., M. Teslenko, P. van der Mark, D. L. Ayres, A. Darling, S. Hohna, B. Larget, L. Liu, M. A.
585   Suchard, and J. P. Huelsenbeck. 2012. MrBayes 3.2: efficient Bayesian phylogenetic inference and
586   model choice across a large model space. Systematic Biology **61**:539-542.
587 Roques, A., R. Bellanger, J. B. Daubrée, C. Ducatillon, T. Urvois, and M.-A. Auger-Rozenberg. 2019. Les
588   scolytes exotiques : une menace pour le maquis. Phytoma **727**:16-20.
589 Rugman-Jones, P. F., M. Au, V. Ebrahimi, A. Eskalen, C. Gillett, D. Honsberger, D. Husein, M. G. Wright, F.
590   Yousuf, and R. Stouthamer. 2020. One becomes two: second species of the *Euwallacea fornicatus*
591   (Coleoptera: Curculionidae: Scolytinae) species complex is established on two Hawaiian islands.
592   PeerJ **8**:e9987.
593 Samuelson, G. A. 1981. A synopsis of Hawaiian Xyleborini (Coleoptera: Scolytidae). Pacific Insects **23**:50-
594   92.
595 Sardain, A., E. Sardain, and B. Leung. 2019. Global forecasts of shipping traffic and biological invasions to
596   2050. Nature Sustainability **2**:274-282.
597 Schedl, K. E. 1953. Fauna Madagascariensis - III. Pages 67-106 Mémoires de l'Institut Scientifique de
598   Madagascar - Série E - Tome III.
599 Schrieber, K., and S. Lachmuth. 2017. The genetic paradox of invasions revisited: the potential role of
600   inbreeding x environment interactions in invasion success. Biological Reviews of the Cambridge
601   Philosophical Society **92**:939-952.
602 Seebens, H., T. M. Blackburn, E. E. Dyer, P. Genovesi, P. E. Hulme, J. M. Jeschke, S. Pagad, P. Pyšek, M.
603   Winter, M. Arianoutsou, S. Bacher, B. Blasius, G. Brundu, C. Capinha, L. Celesti-Grapow, W.
604   Dawson, S. Dullinger, N. Fuentes, H. Jager, J. Kartesz, M. Kenis, H. Kreft, I. Kuhn, B. Lenzner, A.
605   Liebhold, A. Mosena, D. Moser, M. Nishino, D. Pearman, J. Pergl, W. Rabitsch, J. Rojas-Sandoval,
606   A. Roques, S. Rorke, S. Rossinelli, H. E. Roy, R. Scalera, S. Schindler, K. Stajerova, B. Tokarska-
607   Guzik, M. van Kleunen, K. Walker, P. Weigelt, T. Yamanaka, and F. Essl. 2017. No saturation in the
608   accumulation of alien species worldwide. Nature Communications **8**:14435.
609 Simberloff, D., J. L. Martin, P. Genovesi, V. Maris, D. A. Wardle, J. Aronson, F. Courchamp, B. Galil, E.
610   Garcia-Berthou, M. Pascal, P. Pyšek, R. Sousa, E. Tabacchi, and M. Vila. 2013. Impacts of biological
611   invasions: what's what and the way forward. Trends in Ecology and Evolution **28**:58-66.
612 Sire, L., D. Gey, R. Debruyne, T. Noblecourt, F. Soldati, T. Barnouin, G. Parmain, C. Bouget, C. Lopez-
613   Vaamonde, and R. Rougerie. 2019. The challenge of DNA barcoding saproxylic beetles in natural
614   history collections - Exploring the potential of parallel multiplex sequencing with Illumina MiSeq.
615   Frontiers in Ecology and Evolution **7**.
616 Sloan, D. B., J. C. Havird, and J. Sharbrough. 2017. The on-again, off-again relationship between
617   mitochondrial genomes and species boundaries. Molecular Ecology **26**:2212-2236.
618 Smith, S. M., and A. I. Cognato. 2022. New non-native pseudocryptic *Cyclorhipidion* species (Coleoptera:
619   Curculionidae: Scolytinae: Xyleborini) found in the United States as revealed in a multigene
620   phylogeny. Insect Systematics and Diversity **6**.
621 Smith, S. M., D. F. Gomez, R. A. Beaver, J. Hulcr, and A. I. Cognato. 2019. Reassessment of the species in
622   the *Euwallacea fornicatus* (Coleoptera: Curculionidae: Scolytinae) complex after the rediscovery of
623   the "lost" type specimen. Insects **10**.
624 Stamatakis, A. 2014. RAxML version 8: a tool for phylogenetic analysis and post-analysis of large
625   phylogenies. Bioinformatics **30**:1312-1313.
626 Storer, C., A. Payton, S. McDaniel, B. Jordal, and J. Hulcr. 2017. Cryptic genetic variation in an inbreeding
627   and cosmopolitan pest, *Xylosandrus crassiusculus*, revealed using ddRADseq. Ecology and
628   Evolution **7**:10974-10986.
629 Stouthamer, R., P. Rugman-Jones, P. Q. Thu, A. Eskalen, T. Thibault, J. Hulcr, L.-J. Wang, B. H. Jordal, C.-Y.
630   Chen, M. Cooperband, C.-S. Lin, N. Kamata, S.-S. Lu, H. Masuya, Z. Mendel, R. Rabaglia, S.
631   Sanguansub, H.-H. Shih, W. Sittichaya, and S. Zong. 2017. Tracing the origin of a cryptic invader:

632   phylogeography of the *Euwallacea fornicatus* (Coleoptera: Curculionidae: Scolytinae) species
633   complex. Agricultural and Forest Entomology **19**:366-375.
634   Tang, J., K. Mao, H. Zhang, X. Xu, X. Xu, H. Guo, and B. Li. 2022. Multiple introductions and genetic
635   admixture facilitate the successful invasion of *Plantago virginica* into China. Biological Invasions.
636   Toews, D. P. L., and A. Brelsford. 2012. The biogeography of mitochondrial and nuclear discordance in
637   animals. Molecular Ecology **21**:3907-3930.
638   UNCTAD. 2020. Review of maritime transport 2020. United Nations, Geneva.
639   Urvois, T., C. Perrier, A. Roques, L. Sauné, C. Courtin, Y. Li, A. J. Johnson, J. Hulcr, M.-A. Auger-
640   Rozenberg, and C. Kerdelhué. 2022. A first inference of the phylogeography of the worldwide
641   invader *Xylosandrus compactus* Journal of Pest Science **95**:1217-1231.
642   Vanderpool, D., R. R. Bracewell, and J. P. McCutcheon. 2018. Know your farmer: ancient origins and
643   multiple independent domestications of ambrosia beetle fungal cultivars. Molecular Ecology
644   **27**:2077-2094.
645   Weir, B. S., and C. C. Cockerham. 1984. Estimating F-statistics for the analysis of population structure.
646   Evolution **38**:1358-1370.
647   Wickham, H. 2016. ggplot2: Elegant graphics for data analysis. Springer-Verlag New York.
648   Wright, S. 1951. The genetical structure of populations. Annals of Eugenics **15**:323-354.
649   Zheng, X. 2013. Statistical prediction of HLA alleles and relatedness analysis in genome-wide association
650   studies. University of Washington, Washington.
651   Zheng, X., D. Levine, J. Shen, S. M. Gogarten, C. Laurie, and B. S. Weir. 2012. A high-performance
652   computing toolset for relatedness and principal component analysis of SNP data. Bioinformatics
653   **28**:3326-3328.
654

Data accessibility

656   Individual RAD sequences files are available in a fq.gz format a the Sequence Read Archive (SRA)

657   (Study Accession no. XXXXX). The VCF files XXXXX.vcf as well as the popmap used in

658   STACKS'population modile and specimens metadata (e.g. GPS coordinates) are available on Portail Data

659   INRAE (XXXXX). The Genbank accession numbers for the mitochondrial haplotypes reported in this paper

660   are XXXXX to XXXXX.

661

Author contribution statement

663   Marie-Anne Auger-Rozenberg and Carole Kerdelhué designed the study. Laure Sauné, Claudine

664   Courtin and Teddy Urvois completed the molecular biology work. Teddy Urvois and Charles Perrier

665   performed the bioinformatics, the statistical analysis and made the figures. Alain Roques, Jiri Hulcr, Hisashi

666   Kajimura and Anthony I. Cognato performed the field work and helped interpret the results. Teddy Urvois,

667   Carole Kerdelhué, Marie-Anne Auger-Rozenberg and Charles Perrier wrote the original draft of the

668   manuscript. All authors reviewed, edited and approved the final version of the manuscript.

669

670   Conflict of interst

671   The authors declare no conflict of interests. Specimens sampled did not involve endangered nor

672   protected species.

673

674   Funding

681

Table 1: Summary of the localities sampled and specimens used in the COI and RAD sequencing analyses. UFFE is short for University of Florida's Forest Entomology Laboratory and uffeID represents the sample's unique identifier in the UFFE collection database. PACA is short for the French region Provence-Alpes-Côtes d'Azur. The complete table featuring the latitude and the longitude of the different localities is available in Supplementary Figure 1.

Sender (Genbank/accession number/uffeID)	Country	Locality	No. in COI analysis (haplotype)	Haplotype diversity	Nucleotide diversity	Mitochondrial cluster	No. In RAD analysis (major genomic group)
Genbank (KX685266.1)	Argentina	-	1 (A02)	-	-	2	-
From Storer et al. 2017	Cameroon	Limbe	-	-	-	1	-
Genbank (MF637141.1)	Canada	Point Pelee National Park	1 (A02)	-	-	2	-
UFFE (19842)	China	Gushan	1 (A04)	-	-	2	1 (4)
UFFE (19847)	China	Nanan	1 (E09)	-	-	1	1 (9)
UFFE (19844)	China	Qishan	1 (E02)	-	-	1	1 (9)
UFFE (19848, 19851)	China	Shiwandashan	2 (A11, E06)	1	0.1093	1, 2	3 (4,9)
UFFE (19722)	China	Hainan	5 (E01, E09)	0.4	0.0113	1	6 (9)
Genbank (MN620075.1)	China	Hong Kong	1 (E06)	-	-	1	-
UFFE (19878)	China	Kadoorie Farm	1 (E06)	-	-	1	1 (9)
UFFE (19877)	China	Tai Po Kau	3 (E06)	0	0	1	7 (9)
INRAE team	China	Wuhan	4 (A11, A12)	0.5	0.0044	2	-
INRAE team	China	Xiangshan	1 (E03)	-	-	1	1 (9)
Genbank (MN620076.1)	China	Shanghai	1 (A10)	-	-	2	-
Anthony Cognato	China	-	2 (D06, D07)	1	0.0018	1	5 (6)
From Storer et al. 2017	China	Xishuangbanna	-	-	-	1	-
Jhunior Morillo	Costa-Rica	Osa Peninsula	-	-	-	-	1 (5)
UFFE (19874)	France	Carrefour de Gallion	4 (D03)	0	0	1	5 (7)
Genbank (KX055193.1, KX055195.1, KX055196.1)	France	Mont Marau	3 (D02)	0	0	1	-
Genbank (KX055198.1)	France	Moorea Island	1 (D02)	-	-	1	-
Genbank (KX055192.1)	France	Motu Tiahura	1 (D02)	-	-	1	-
Genbank (KX055197.1)	France	Tahiti Island	1 (D02)	-	-	1	-
INRAE team	France	Bayonne	1 (A10)	-	-	2	-
INRAE team	France	Saint Jean de Luz	2 (A03)	0	0	2	2 (5)
INRAE team	France	Saint Maurice sur Adour	2 (A03)	0	0	2	5 (4)
INRAE team	France	Gignac	1 (A10)	-	-	2	1 (5)
INRAE team	France	Cap d'Ail	5 (A10)	0	0	2	3 (5)
INRAE team	France	Cap Ferrat	1 (A10)	-	-	2	2 (5)
INRAE team	France	Menton	1 (A10)	-	-	2	1 (5)
INRAE team	France	Mont Boron	1 (A10)	-	-	2	4 (5)
Genbank (MN182983.1, MN183016.1)	France	Nice	2 (A10)	0	0	2	-
INRAE team	France	Nice Albert 1er	2 (A10)	0	0	2	2 (5)
INRAE team	France	Nice Vallée du Var	1 (A10)	-	-	2	1 (4)
INRAE team	France	Sainte-Marguerite	3 (A10)	0	0	2	3 (5)
INRAE team	France	Villa Thuret	7 (A10)	0	0	2	5 (5)
From Storer et al. 2017	Ghana	Ankasa	-	-	-	1	-
From Storer et al. 2017	Honduras	-	-	-	-	2	-
Genbank (MN620071.1)	India	Dehra Dun	1 (D01)	-	-	1	-
UFFE (7942)	Indonesia	Bangunrejo	2 (D02)	0	0	1	5 (7)
UFFE (7954)	Indonesia	Blawan	2 (D02)	0	0	1	5 (7)
INRAE team	Italy	Parco Monti Aurunci	3 (A02)	0	0	2	5 (4)
INRAE team	Italy	Parco Riviera di Ulisse	2 (A02)	0	0	2	2 (4)
INRAE team	Italy	Sabaudia	3 (A02)	0	0	2	5 (3)
Hisashi Kajimura	Japan	Amami	2 (A02, C04)	1	0.0705	2	1 (2)
From Ito & Kajimura 2009	Japan	Amami	-	-	-	2	-
Hisashi Kajimura	Japan	Okinawa, Naha	3 (A07, C05, C06)	1	0.0470	2	3 (2,4)
From Ito & Kajimura 2009	Japan	Naha	-	-	-	2	-
From Storer et al. 2017	Japan	Aichi	-	-	-	2	-
From Ito & Kajimura 2009	Japan	Nagano, Chiisagata-gun	-	-	-	2	-
Hisashi Kajimura	Japan	Nagano, Chiisagata-gun	2 (B06, B07)	1	0.0018	2	2 (1)
From Ito & Kajimura 2009	Japan	Nagano, Shimominochi-gun	-	-	-	2	-
From Ito & Kajimura 2009	Japan	Nagano, Shiojiri	-	-	-	2	-
Hisashi Kajimura	Japan	Tottori	2 (A02)	0	0	2	2 (3)
From Ito & Kajimura 2009	Japan	Tottori	-	-	-	2	-
Hisashi Kajimura	Japan	Hiroshima, Miyoshi	2 (A02, B02)	1	0.0705	2	2 (1,3)
From Ito & Kajimura 2009	Japan	Hiroshima, Miyoshi	-	-	-	2	-
Hisashi Kajimura	Japan	Sapporo	2 (B03, B05)	1	0.0053	2	2 (1)
From Ito & Kajimura 2009	Japan	Sapporo	-	-	-	2	-
From Ito & Kajimura 2009	Japan	Toyama, Nakashinkawa-gun	-	-	-	2	-
From Ito & Kajimura 2009	Japan	Saitama, Chichibu	-	-	-	2	-
From Ito & Kajimura 2009	Japan	Chiba, Kamogawa	-	-	-	2	-
From Ito & Kajimura 2009	Japan	Kyoto, Maizuru	-	-	-	2	-
From Ito & Kajimura 2009	Japan	Kyoto, Nantan	-	-	-	2	-
From Ito & Kajimura 2009	Japan	Mie, Isshi-gun	-	-	-	2	-
From Ito & Kajimura 2009	Japan	Wakayama, Tanabe	-	-	-	2	-
From Ito & Kajimura 2009	Japan	Miyakazi, Kobayashi	-	-	-	2	-
Hisashi Kajimura	Japan	Miyakazi, Kobayashi	-	-	-	-	1 (1)
Genbank (MN620077.1)	Japan	Okinawa	1 (D02)	-	-	1	-
Hisashi Kajimura	Japan	Koshi, Hata-gun	2 (B01, B02)	1	0.0035	2	3 (1)
From Ito & Kajimura 2009	Japan	Koshi, Hata-gun	-	-	-	2	-
From Storer et al. 2017	Japan	Iriomote	-	-	-	2	-
Hisashi Kajimura	Japan	Ishigaki	3 (C01, C02, C03)	1	0.0035	2	3 (2)
From Ito & Kajimura 2009	Japan	Ishigaki	-	-	-	2	-
From Ito & Kajimura 2009	Japan	Iwate, Iwate-gun	-	-	-	2	-
Hisashi Kajimura	Japan	Yamagata, Tsuruoka	3 (B04, B05)	0.667	0.0012	2	2 (1)
From Ito & Kajimura 2009	Japan	Yamagata, Tsuruoka	-	-	-	2	-
Hisashi Kajimura	Japan	Shizuoka	2 (A02)	0	0	2	2 (3)
From Ito & Kajimura 2009	Japan	Shizuoka	-	-	-	2	-
From Ito & Kajimura 2009	Japan	Aichi, Toyota	-	-	-	2	-
Genbank (GU808709.1)	Madagascar	-	1 (D02)	-	-	1	-
From Storer et al. 2017	Madagascar	Ranomafana	-	-	-	1	-
Ben Boyd	New Zealand	Auckland	4 (A02)	0	0	2	5 (3)
Genbank (KX035196.1)	Panama	-	2 (D04)	0	0	1	-
Anthony Cognato	Panama	Barro Colorado Island	2 (D04)	0	0	1	5 (5)
UFFE (19876)	Papua New	Kugofanka	4 (A02, D02)	0.5	0.0547	1, 2	5 (3,8)

|							
	Guinea						
From Storer et al. 2017	Papua New Guinea	Madang	-	-	-	1	-
UFFE (19863, 19864, 19865, 19866, 19867)	Papua New Guinea	Ohu	2 (D10)	0	0	1	5 (7)
Andreja Kavčič	Slovenia	Podsabotin	16 (A09, A10)	0.233	0.0025	2	5 (4)
From Nel et al. 2020	South Africa	-	-	-	-	1	-
From Nel et al. 2020	South Africa	Tzaneen	3 (A06)	0	0	2	-
From Nel et al. 2020	South Africa	-	1 (D04)	-	-	1	-
Diego Gallego	Spain	El Tello	12 (A02)	0	0	2	5 (3)
Diego Gallego	Spain	Naquera	2 (A02)	0	0	2	5 (3)
UFFE (8515, 8520)	Taiwan	Dayueshan	2 (E03)	0	0	1	3 (7,9)
From Storer et al. 2017	Taiwan	Dali	-	-	-	1, 2	-
Genbank (MN620074.1)	Taiwan	-	1 (E10)	-	-	1	-
Genbank (GU808708.1)	Thailand	-	1 (D05)	-	-	1	-
From Storer et al. 2017	Thailand	Doi Pui	-	-	-	1	-
Genbank (BBCCA4264-12)	USA	Toad Suck Park	1 (A02)	-	-	2	-
Genbank (BBCCA4147-12C)	USA	Collier Seminole State Park	1 (A06)	-	-	2	-
Jared Bernard	USA	Manoa Valley	4 (A01, A02, D02)	0.833	0.0738	1, 2	5 (3,7)
Jared Bernard	USA	Moloa'a Bay	4 (A02, A10)	0.667	0.0129	2	4 (7)
Jared Bernard	USA	Poamoho Ridge	3 (A05, D02)	0.667	0.0670	1, 2	2 (4,7)
Anthony Cognato	USA	Vulcano Nat. Park	2 (A02)	0	0	2	5 (7)
Genbank (GU808710.1)	USA	-	1 (A02)	-	-	2	-
Jhunior Morillo	USA	Long Island	2 (A02)	0	0	2	2 (3)
Anthony Cognato	USA	Smithtown	2 (A02)	0	0	2	2 (3)
Genbank (GU808711.1)	USA	-	1 (A02)	-	-	2	-
UFFE (20193)	USA	Cherokee	2 (A02)	0	0	2	5 (3)
Steve Frank	USA	Raleigh	4 (A02, A07)	0.5	0.0071	2	3 (3,4)
UFFE (17525, 17526)	USA	Leone	8 (D02, D03)	0.25	0.0004	1	5 (7)
UFFE (20230)	USA	Cosby	2 (A02)	0	0	2	5 (3)
Genbank (GMGSC323-12)	USA	Great Smoky Mountains Nat. Park	1 (A02)	-	-	2	-
Anthony Cognato	USA	Tomball	2 (A02, A08)	0	0	2	5 (3,4)
Anthony Cognato	Vietnam	-	2 (E07, E12)	1	0.0071	1	2 (9)
Genbank (MN620070.1)	Vietnam	-	1 (E11)	-	-	1	-
Anthony Cognato	Vietnam	Cát Tiên Nat. Park	2 (D09)	0	0	1	5 (8)
Genbank (MN620073.1)	Vietnam	Cát Tiên National Park	1 (D08)	-	-	1	-
Anthony Cognato	Vietnam	-	1 (E15)	-	-	1	4 (9)
Genbank (MN620078.1)	Vietnam	-	1 (E08)	-	-	1	-
Anthony Cognato	Vietnam	-	2 (E09)	0	0	1	3 (9)
Genbank (MN620072.1)	Vietnam	-	1 (E09)	-	-	1	-
UFFE (14645)	Vietnam	Tam Dao	15 (E04, E05, E13, E14)	0.467	0.0041	1	5 (9)
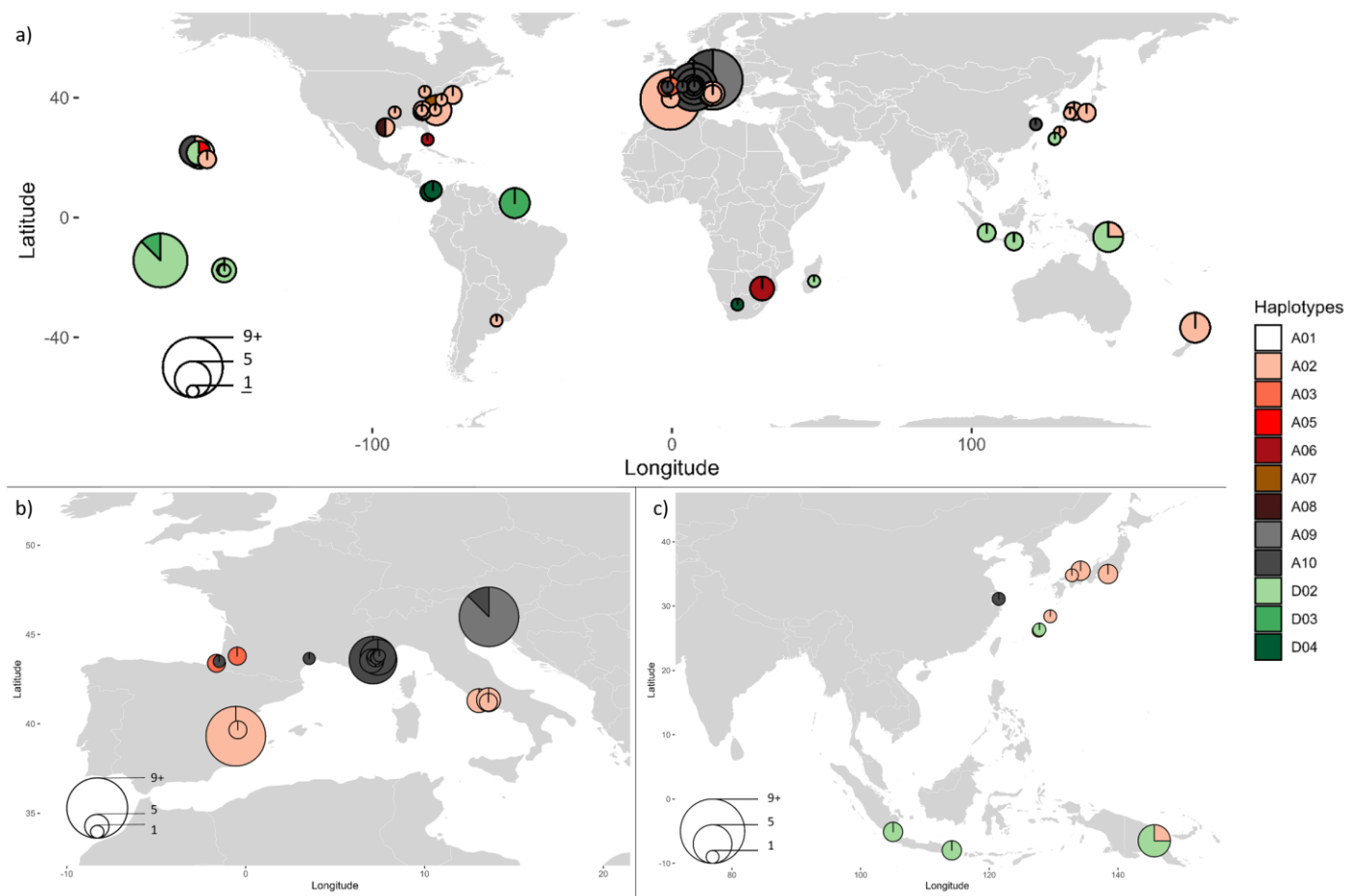
Figure 1: X. crassiusculus *' invasive haplotype map a) worldwide; b) focusing on Europe, and c) and focusing on Asia. The coordinates of some localities were not known (cf. Table 1). Their pies were thus added at approximate coordinates.*

684

Table 2: Genetic distances within and between COI lineages (derived from the mitochondrial haplotypes) and their respective standard error estimates based on the Kimura 2-parameter model. The genetic distances between COI lineages are on the bottom left part, and the standard error estimates on the top left part of the table.

685

	Within		Between				
	Distances	Standard Error Estimates	Lineage A	Lineage B	Lineage C	Lineage D	Lineage E
Lineage A	0.0135	0.003		0.011	0.0117	0.0123	0.014
Lineage B	0.0076	0.0024	0.0709		0.0128	0.0135	0.0147
Lineage C	0.014	0.0039	0.0798	0.0932		0.0135	0.0145
Lineage D	0.0482	0.0063	0.1095	0.1242	0.1158		0.01
Lineage E	0.0152	0.0029	0.1176	0.1252	0.1188	0.0783	

686

687

	Genomic group 1	Genomic group 2	Genomic group 3	Genomic group 4	Genomic group 5	Genomic group 6	Genomic group 7	Genomic group 8	Genomic group 9
Genomic group 1	0	0,403	0,383	0,375	0,38	0,368	0,373	0,384	0,37
Genomic group 2	0,899	0	0,328	0,321	0,327	0,381	0,382	0,388	0,381
Genomic group 3	0,948	0,96	0	0,013	0,024	0,358	0,364	0,37	0,363
Genomic group 4	0,907	0,923	0,411	0	0,019	0,362	0,375	0,371	0,364
Genomic group 5	0,939	0,969	0,671	0,504	0	0,359	0,369	0,371	0,363
Genomic group 6	0,913	0,957	0,965	0,94	0,977	0	0,075	0,126	0,108
Genomic group 7	0,943	0,962	0,961	0,949	0,967	0,855	0	0,12	0,102
Genomic group 8	0,928	0,965	0,968	0,947	0,979	0,919	0,906	0	0,081
Genomic group 9	0,912	0,93	0,949	0,926	0,947	0,8	0,83	0,768	0

695 *Table 3: Fst (bottom left part) and Nei (top left part) distances between genomic groups.*

696
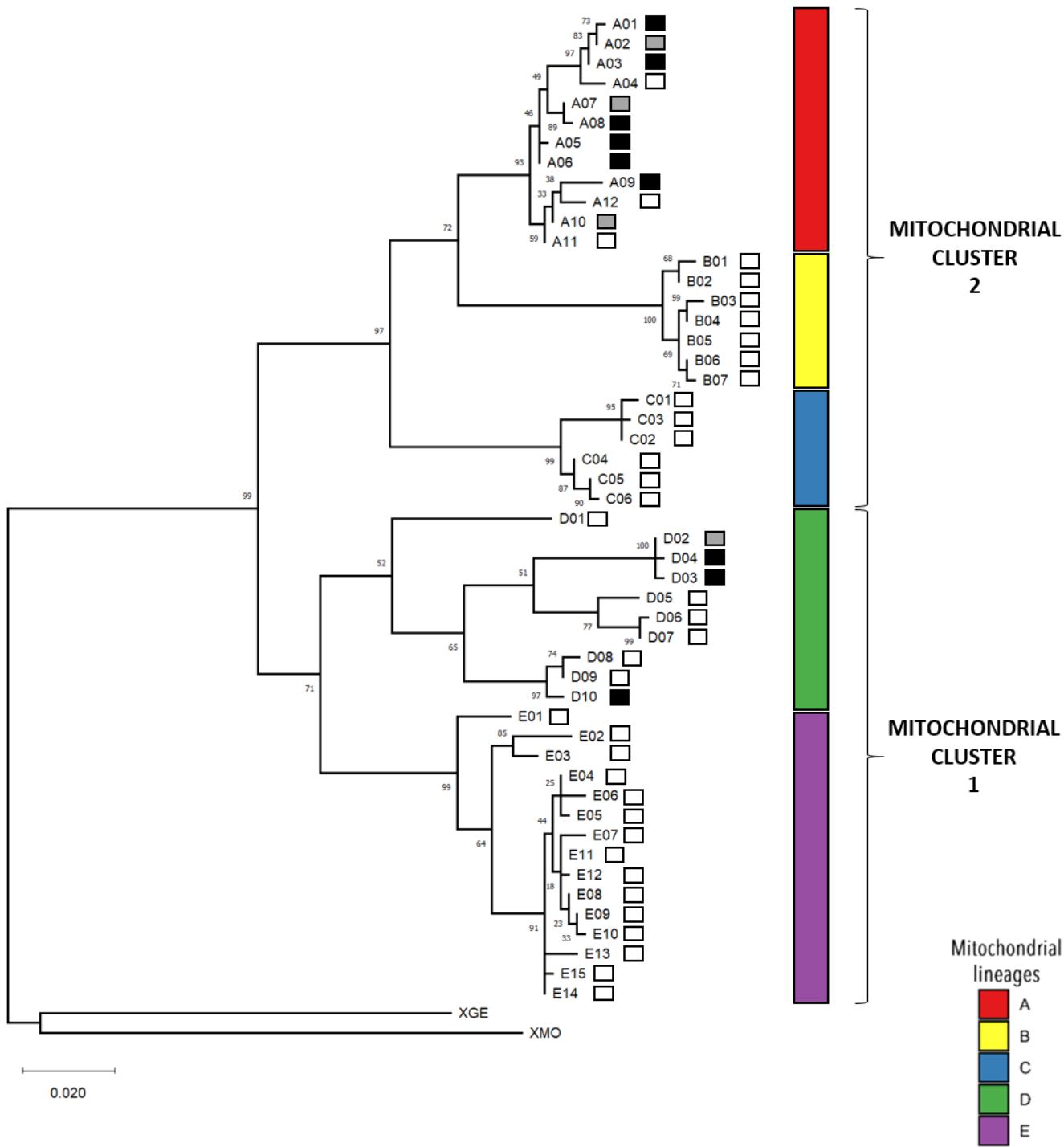
Figure 2: Maximum Likelihood tree based on X. crassiusculus *'COI sequences built with MEGA X. We used* Xylosandrus germanus *(XGE NC036280.1) and* Xylosandrus morigerus *(XMO NC_036283.1) as outgroups. The color of the squares next to the haplotypes shows whether they were identified in the native area only (white), in the invaded area only (black) or in both areas (grey).*
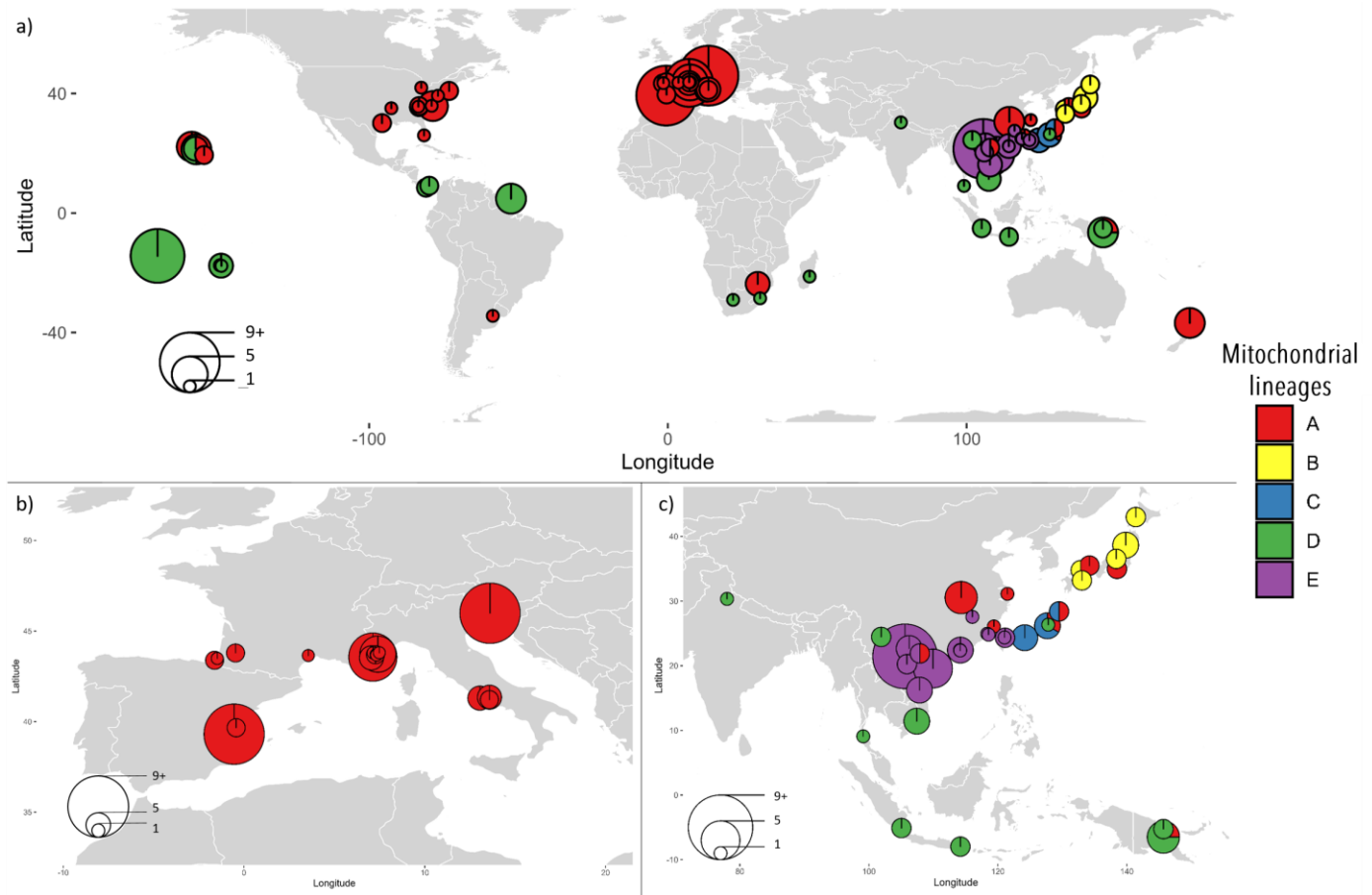
697

Figure 3: X. crassiusculus *' mitochondrial lineage map a) worldwide ; b) focusing on Europe, and c) focusing on Asia. The coordinates of some localities were not known (cf. Table 1). Their pies were thus added at approximate coordinates. The mitochondrial lineages were derived from mitochondrial the haplotypes.*
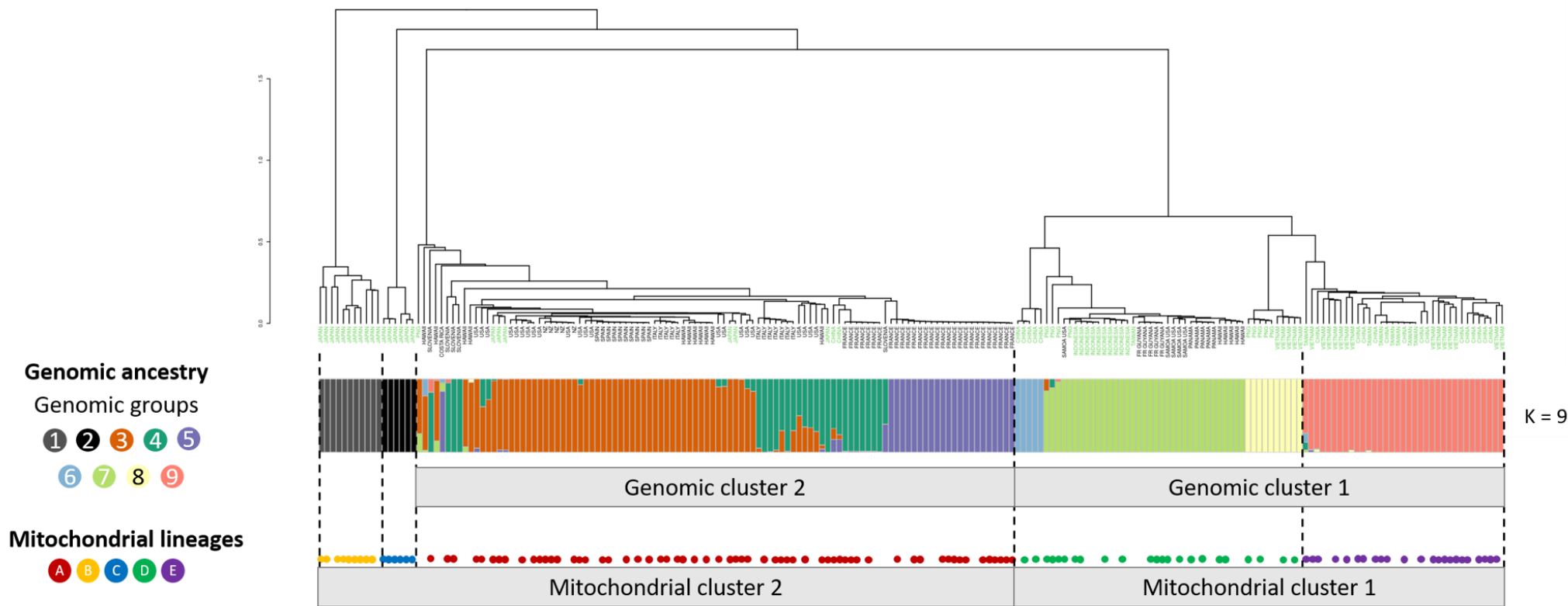
Figure 4: Clustering tree and admixture plot for K = 9 calculated on Xylosandrus crassiusculus' RAD sequencing data. The leaves labels of the clustering tree represent the country of origin of the samples, and the countries in the X. crassiusculus' native area are represented in green. When available, the specimens' mitochondrial lineage, derived from the mitochondrial haplotypes, are represented as colored circles at the bottom of the figure.
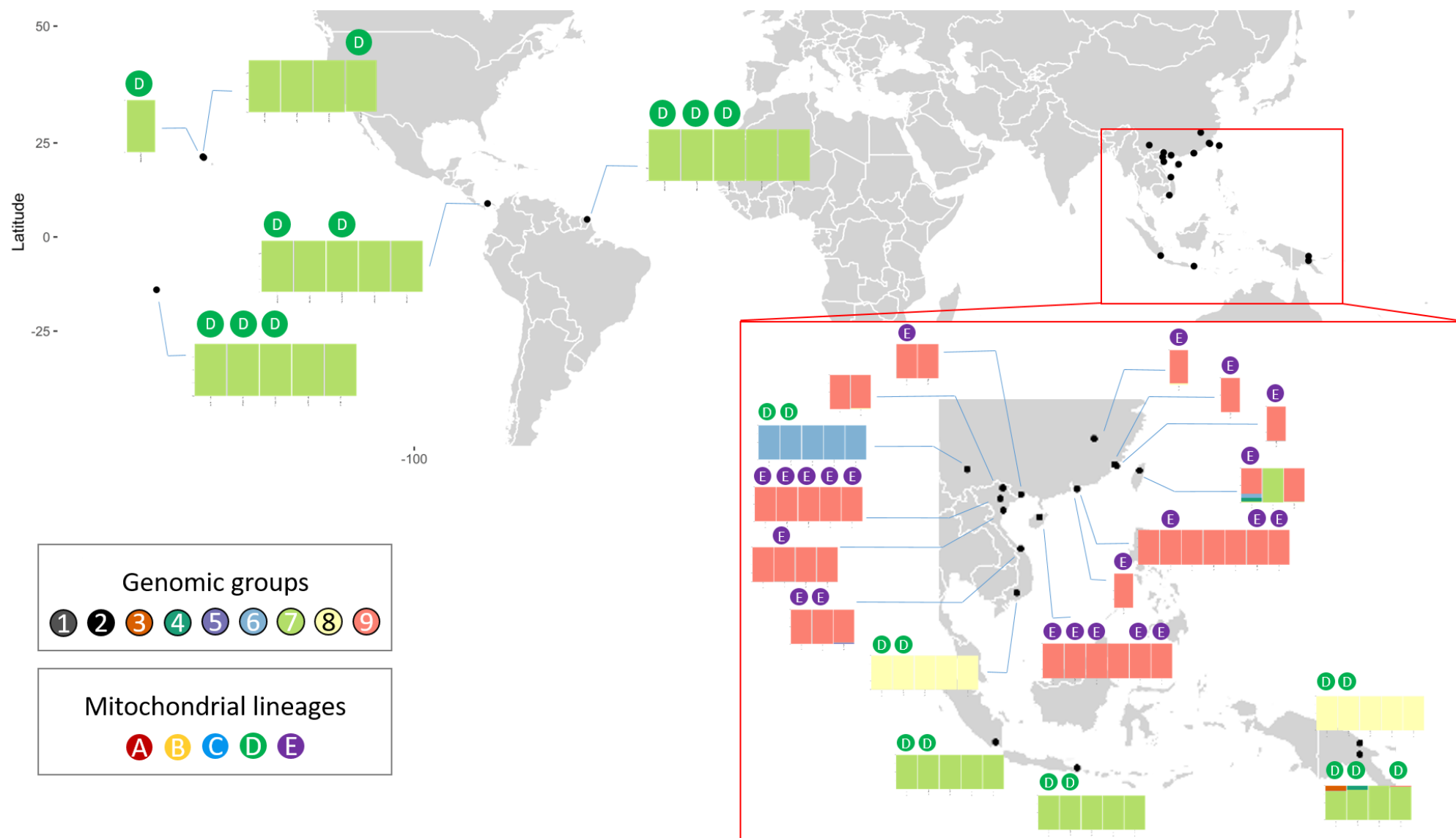
Figure 5: Map representing the admixtures plot for the specimens belonging to the genomic cluster 1. The specimens' mitochondrial lineage, derived from its mitochondrial haplotype, was added on top of the barplots when available.
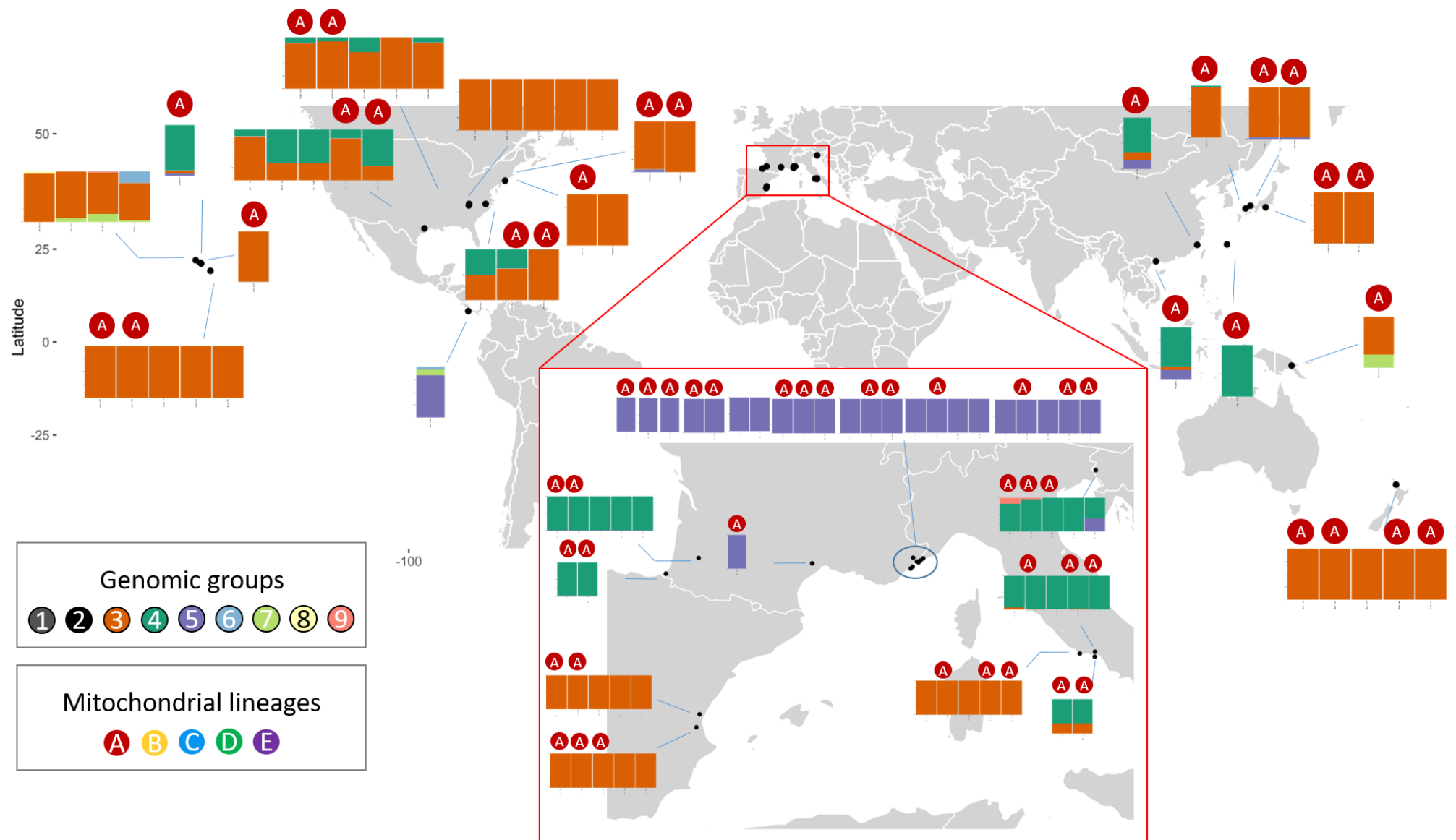
Figure 6: Map representing the admixtures plot for the specimens belonging to the genomic cluster 2. The specimens' mitochondrial lineage, derived from its mitochondrial haplotype, was added on top of the barplots when available.
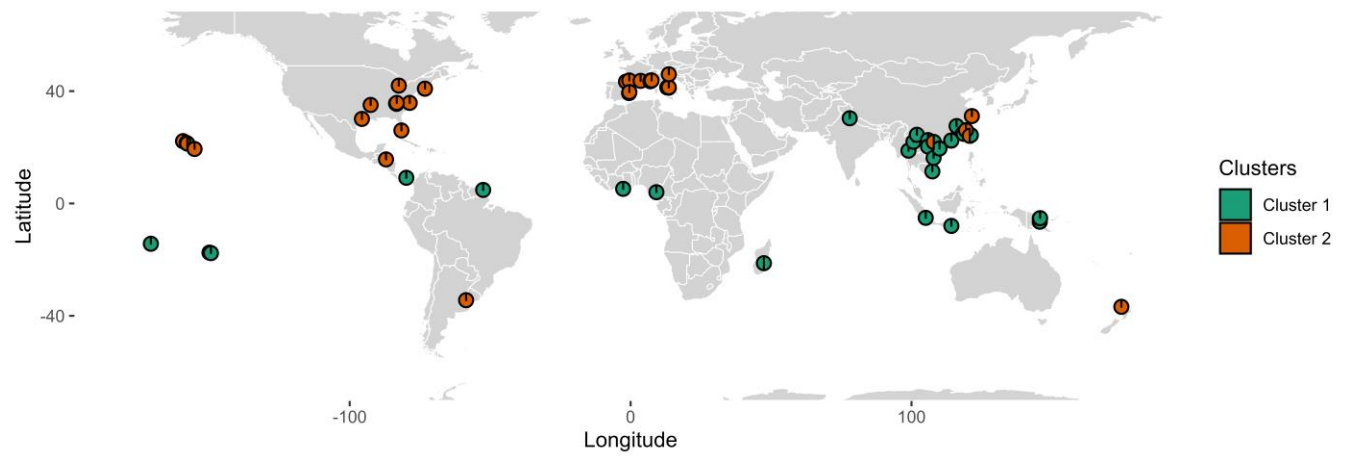
Figure 7: Map representing the worldwide distribution of the two genomic Clusters of X. crassiusculus.

703

704

Figure 8: Potential invasion scenarios of Xylosandrus crassiusculus in the USA, Canada, Argentina and Europe.

705